

Article

## Imaging Velocimetry Measurements for Entropy Production in a Rotational Magnetic Stirring Tank and Parallel Channel Flow

Greg F. Naterer <sup>1,\*</sup> and Olusola B. Adeyinka <sup>2</sup>

<sup>1</sup> University of Ontario Institute of Technology, Oshawa, Ontario, L1H 7K4, Canada;

E-mail: greg.naterer@uoit.ca

<sup>2</sup> Imperial Oil Resources, Calgary, Alberta, T2L 2K8, Canada; E-mail: olusola.b.adeyinka@esso.ca

\* Author to whom correspondence should be addressed.

Received: 3 July 2009 / Accepted: 19 July 2009 / Published: 23 July 2009

---

**Abstract:** An experimental design is presented for an optical method of measuring spatial variations of flow irreversibilities in laminar viscous fluid motion. Pulsed laser measurements of fluid velocity with PIV (Particle Image Velocimetry) are post-processed to determine the local flow irreversibilities. The experimental technique yields whole-field measurements of instantaneous entropy production with a non-intrusive, optical method. Unlike point-wise methods that give measured velocities at single points in space, the PIV method is used to measure spatial velocity gradients over the entire problem domain. When combined with local temperatures and thermal irreversibilities, these velocity gradients can be used to find local losses of energy availability and exergy destruction. This article focuses on the frictional portion of entropy production, which leads to irreversible dissipation of mechanical energy to internal energy through friction. Such effects are significant in various technological applications, ranging from power turbines to internal duct flows and turbomachinery. Specific problems of a rotational stirring tank and channel flow are examined in this paper. By tracking the local flow irreversibilities, designers can focus on problem areas of highest entropy production to make local component modifications, thereby improving the overall energy efficiency of the system.

**Keywords:** entropy production; particle image velocimetry

---

## Nomenclature

$F_b$	body force (N/m <sup>3</sup> )
$g$	gravitational acceleration (m/s <sup>2</sup> )
$h_l$	head loss (m <sup>2</sup> /s <sup>2</sup> )
$i, j$	PIV grid point (row, column number)
$p$	pressure (kPa)
$\dot{P}_s$	volumetric entropy production rate (W/m <sup>3</sup> K)
$q$	heat flux (W/m <sup>2</sup> )
$s$	specific entropy (J/kgK) or streamwise coordinate
$t$	time (s)
$T$	temperature (K)
$u, v$	components of velocity (m/s)
$V$	total velocity magnitude (m/s)
$x, y$	Cartesian coordinates (m)

## Greek

$\rho$	density (kg/m <sup>3</sup> )
$\mu$	dynamic viscosity (kg/ms)
$\tau$	stress tensor (N/m <sup>2</sup> )

## 1. Introduction

From engineering fluid mechanics, to information/coding theory, economics and biology, the many applications of entropy are widespread. Entropy serves as a key parameter in reaching the upper limits of performance and quality in many engineering technologies. It can shed new light on various flow processes, ranging from optimized flow configurations in an aircraft engine, to highly ordered crystal structures (low entropy) in a turbine blade, and other applications [1,2]. It is likely not possible to find any other law of nature, whereby a proposed violation would bring more skepticism than violation of the Second Law.

An important example of entropy-based design is the optimized flow design of aircraft sub-systems, involving work potential [3]. Currently there is no systematic method for tracking work potential usage in the design of aircraft sub-systems [4]. Exergy and entropy calculations can identify the loss of work potential within each sub-system and fluid flow process during an aircraft's operation. This would provide the designer with a systematic way of identifying and targeting those areas incurring the most significant losses. In this way, economic decisions could be directly linked to work potential and flow irreversibilities. Moorhouse and Suchomel [5] reported that flow exergy provides a unifying framework and a set of metrics to more effectively analyze aircraft sub-systems.

Another important application of entropy-based design arises with thermal management of electronic devices. Optimized convective cooling of microelectronic assemblies has received considerable past attention. The effects of component layout on flow patterns in such assemblies were

investigated in a water tunnel by Azar and Russell [6]. Flow visualization can be performed in water tunnels with pulsed laser illumination and Particle Image Velocimetry [7,8]. Entropy generation has been used to find the minimum power input for convective cooling of an electronic package [9]. The minimization is carried out with respect to the coolant flow rate and heat transfer contact area. Landauer [10] outlined how the ultimate physical limitations on faster and more compact microelectronic circuits can be directly linked to the Second Law.

Recent advances in computational methods have outlined the importance of the Second Law of Thermodynamics in fluid flow analysis. A detailed review of entropy and its significance in CFD (Computational Fluid Dynamics) was presented by Naterer and Camberos [11]. The Second Law provides a quantitative measure of the amount of flow dissipation added and the amount required for accurate CFD simulations [12,13]. Merriam [14] outlined that satisfying the Second Law globally is sufficient, but not necessary, for numerical CFD stability. Naterer [15] showed that the Second Law can be used to assess stability of individual components within an overall CFD formulation. The Second Law can effectively outline a time step size [3] with a symmetric form of the conservation equations [16] for numerical stability in CFD.

In fluid flow simulations, the consequences of inadequate grid or time step refinement may lead to negative entropy production, when formulated in terms of the transport form of the Second Law. Such results have been documented by Adeyinka and Naterer [17], Nellis and Smith [18] and Naterer and Schneider [19]. As a result, an important issue involves which specific mechanisms lead to such solution anomalies, as well as how they can be offset to ensure reliable and physically realistic results. An entropy-based approach can provide well quantified error bounds and better robustness metrics. With such advances, deeper integration of CFD technology into the industrial design process can be realized.

Entropy production of viscous fluid motion leads to pressure losses and other irreversible dissipation of mechanical energy into internal energy. With previous technologies, such losses have generally been characterized globally with a single loss coefficient. In this article, an optical method of entropy production indirect measurement is developed, so that flow irreversibilities and loss coefficients can be tracked locally. In this way, flow devices can be re-designed locally to improve performance. Minimizing this local entropy production could provide a new systematic way of improving energy utilization of complex thermofluid devices.

Flow irreversibility measurements can provide a single common way of characterizing the local losses within any fluid device. Unlike other flow variables such as pressure, entropy production encompasses all types of flow irreversibilities. High entropy production can identify the local problem areas. A useful analogy is a patient telling the doctor that he/she is sick, without knowing the part of the body causing the ailment. It would be more helpful if the patient could identify the problem area, such as a sore lower back, so that the doctor could focus efforts on that body part. Similarly for complex engineering systems, large rates of local entropy production would identify areas of concern, since a commonly desired goal is improving efficiency through reduced entropy production. As industrial technologies become more complex, such measurements can provide competitive advantages in developing new technologies, which would more closely reach the upper limits of performance. As future technologies press towards these upper theoretical limits, it is anticipated that the Second Law will have an increasingly important role therein. In this article, indirect measurements

of local flow irreversibilities will be presented. The technique will provide designers with a useful tool to identify regions of highest entropy production, from which local design modifications can improve overall energy efficiency of the systems.

## 2. Formulation of Flow Irreversibilities and Entropy Production

The Second Law of Thermodynamics provides vital information for the achievement of various technological goals, as it provides quantitative information about the locations of irreversible flow losses. Unlike the conservation equations, the Second Law represents an inequality, rather than an equality. The transport form of the Second Law may be written as:

$$\frac{\partial(\rho s)}{\partial t} + \nabla \cdot \left( \rho \bar{v} s + \frac{\bar{q}}{T} \right) = \dot{P}_s \quad (1)$$

where  $\rho$ ,  $s$ ,  $v$ ,  $q$  and  $\dot{P}_s$  refer to the fluid density, entropy, velocity, Fourier heat flux and entropy production rate, respectively. For irreversible processes such as viscous fluid mixing, the Second Law requires that the entropy production rate is positive. This entropy production arises from the irreversible degradation of mechanical energy into internal energy through viscous dissipation, as well as heat transfer across a finite temperature difference.

The rate of destruction of exergy can be obtained from Equation 1, after multiplying the entropy production rate by local temperature at position (x,y,z). In some ways, exergy can be more readily interpreted physically, as it contains the same dimensional units as energy. Thus, it can be related directly to economic indicators. For example, when a fluid is throttled and its pressure is reduced across a valve, a certain amount of exergy is destroyed in the process. Multiplying the local cost of electricity (per kWhr) by this exergy destroyed over a year can indicate a yearly expense of wasted energy therein, or a measure of lost revenue. It could have been prevented if a local power generator (such as a power turbine) extracted this exergy and converted it to useful energy such as electricity, while the turbine lowered the pressure to the same thermodynamic state on the downstream side of the valve. Since exergy and energy per unit volume have the same dimensional units, economic calculations can be performed relatively quickly.

Flow irreversibilities constitute a source term of the internal energy equation, while simultaneously acting as an energy sink of mechanical energy. The magnitude of flow irreversibility is characterized by the rate of entropy production, which can be written directly in terms of spatial velocity gradients for near-isothermal flows of Newtonian fluids as follows:

$$\dot{P}_s = \frac{\mu}{T} \left\{ \left( \frac{\partial u}{\partial y} + \frac{\partial v}{\partial x} \right)^2 + 2 \left( \left( \frac{\partial u}{\partial x} \right)^2 + \left( \frac{\partial v}{\partial y} \right)^2 \right) \right\} \quad (2)$$

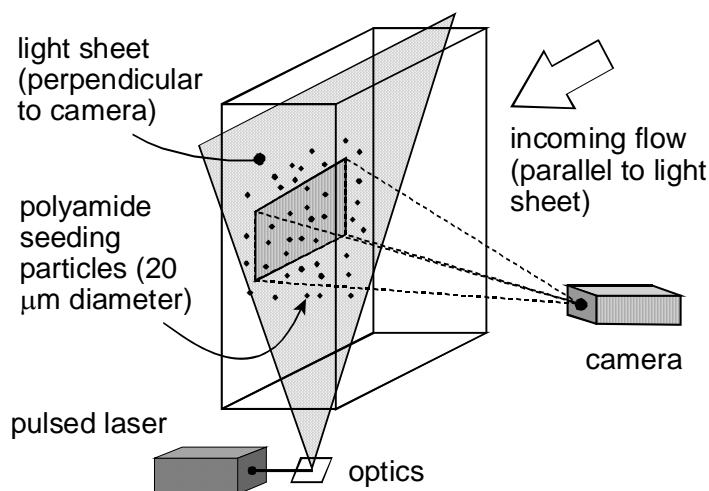
where  $\mu$ ,  $T$ ,  $x$  and  $y$  refer to the dynamic viscosity, temperature and Cartesian coordinates, respectively. The right side of Equation 2 is a sum of squares, and thus the entropy production rate is positive for irreversible processes. The terms remain positive since mechanical energy is continuously degraded to internal energy through viscous dissipation. Although not shown in Equation 2, an additional thermal irreversibility arises for non-isothermal flows, when heat flows irreversibly down a temperature gradient through heat conduction. Both cases produce microscopic disorder (or entropy) in the fluid.

Equations 1 - 2 provide two different alternatives for calculating  $\dot{P}_s$ . The entropy transport equation is designated by Equation 1, whereas the positive definite form is given in Equation 2. Previous studies have shown that the computed  $\dot{P}_s$  in Equation 1 can be directly linked with numerical stability, discretization error and other useful measures [11]. But in this article,  $\dot{P}_s$  will be determined from Equation 2 and its spatial integration over a discrete PIV grid. In Equation 1, entropy must be evaluated in terms of temperature through the Gibbs equation, whereas  $\dot{P}_s$  is approximated directly in terms of velocities, temperature and viscosity in Equation 2. The significance of any difference obtained from both approaches has been reported previously by Adeyinka and Naterer [17].

### 3. Experimental Procedure

Unlike velocity or temperature, the measurement of entropy cannot be performed directly. However, Equation 2 can be used in an indirect way to characterize the flow irreversibility. In this paper, the entropy produced by friction irreversibilities will be determined from measured gradients of velocity through Equation 2. These spatial gradients will be obtained from pulsed laser PIV measurements in a water tunnel. A schematic of the experimental setup is illustrated in Figure 1.

**Figure 1.** Experimental setup of particle image velocimetry.



Laminar channel flow experiments were performed in a water tunnel with polyamide seeding particles. Fluid flow measurements were performed sufficiently downstream of the channel entrance, so fluid velocities are known to be fully developed. A planar cross-section in the center of the channel, parallel to the flow and perpendicular to the wall, was illuminated by the pulsed laser. Two successive images were processed to give instantaneous values of both components of fluid velocity ( $u$  and  $v$ ).

Particle Image Velocimetry (PIV) is a well-known technique for measuring whole-field distributions of fluid velocity. In the current study, the seeded particles are illuminated along a plane sheet perpendicular to the camera. The PIV software quantifies distances between groups of particles over successive images and the elapsed time to determine the particle velocities. A Dantec 2100 PIV system was used and steady-state measurements were recorded. The seeding particles within the

parallel plate channel were illuminated at different downstream locations by reflecting optics and a two-chamber Gemini PIV Nd: Yag pulsed laser. Extensive efforts were taken for the near-wall measurements, in view of their significance when calculating peak values of flow irreversibilities near the wall.

The interrogation region of the FlowMap software and camera are centered about the channel flow region within the water tunnel. The PIV images were recorded with a Kodak MegaPlus ES1.0 Type 16 (20 kHz) camera and Dantec HiSense CCD camera. Camera images at two different times were processed, matched and sub-divided into small interrogation regions, in order to determine the displacement of a group of particles (based on FFT correlations). The local fluid velocity was then determined, based on the displacement and elapsed time,

A process for establishing the time between laser pulses was needed to optimize the seeding density. In these studies, the peak height ratio was set to 1 and the velocity length slider was set to 25%. This means that any vectors longer than 25% of the length of the interrogation area were highlighted in red and assumed to be inaccurate. Starting with a very low time between pulses and gradually increasing the time for successive image captures, the velocities in the vector map become smoother and more continuous. The optimum time between pulses was selected. This time interval between pulses was kept constant, so consistent results were gathered throughout tests involving a particular flow configuration. Then, post-processed velocity results were used to find local rates of entropy production. The measured velocity vectors were displayed by the PIV software over a discrete grid. Then,  $\dot{P}_s$  can be determined by spatial differencing of Equation 2 over the discrete grid. Let  $u(i,j)$  and  $v(i,j)$  denote the velocity components at grid position  $(i,j)$ . Based on Equation 2:

$$\begin{aligned} \dot{P}_s = & \frac{\mu}{T(i,j)} \left( \frac{u(i,j+1) - u(i,j-1)}{\Delta y} + \frac{v(i+1,j) - v(i-1,j)}{\Delta x} \right)^2 \\ & + 2 \frac{\mu}{T(i,j)} \left( \left( \frac{u(i+1,j) - u(i-1,j)}{\Delta x} \right)^2 + \left( \frac{v(i,j+1) - v(i,j-1)}{\Delta y} \right)^2 \right) \end{aligned} \quad (3)$$

where  $\Delta x$  and  $\Delta y$  refer to the grid spacing in the  $x$  and  $y$  directions (note: for near-isothermal flow examples in this paper,  $T(i,j)$  is assumed constant).

#### 4. Local Loss Coefficients Based on Flow Exergy

Conventional loss parameters, such as a global head loss or pressure recovery coefficient, cannot identify specific locations and sources of flow losses in fluid systems. The previously developed technique of measured entropy production allows local irreversibilities to be scrutinized and converted to local distributions of the loss coefficient. In this way, a designer could use local loss mapping to detect regions of highest entropy production (or flow irreversibility), thereby allowing local design changes of geometrical or other parameters. In this section, it will be shown that locally measured entropy production can be converted to local loss parameters, thus providing a useful alternative and generalized approach to loss analysis.

Consider incompressible viscous flow through a streamtube in the flow direction, between an inlet (subscript 1) and outlet (subscript 2). The well-known Bernoulli's equation outlines the head loss along this flow path as follows:

$$\frac{p_1}{\rho_1} + gz_1 + \frac{1}{2}V_1^2 = \frac{p_2}{\rho_2} + gz_2 + \frac{1}{2}V_2^2 + h_l \quad (4)$$

where  $h_l$  is the head loss. Also,  $p$ ,  $g$ ,  $z$  and  $V$  refer to pressure, gravitational acceleration, elevation and total velocity, respectively. It can be shown that Bernoulli's equation represents an integrated form of the following differential mechanical energy equation [2]:

$$\rho \frac{D}{Dt} \left( \frac{1}{2} V^2 \right) = -\bar{v} \cdot \nabla p + \nabla \cdot \bar{\tau} \cdot \bar{v} - \tau : \nabla \bar{v} + \bar{F}_b \cdot \bar{v} \quad (5)$$

where  $D/Dt$ ,  $\tau$ ,  $F_b$  and  $v$  refer to the total (substantial) derivative, shear stress tensor, body force and fluid velocity vector, respectively. The colon symbol ( $:$ ) represents matrix contraction between the shear stress and velocity gradient tensors. The temporal part of the substantial derivative on the left side becomes zero under steady state conditions.

The previous equation requires that the net convection of kinetic energy (first term) balances the sum of flow work (second term), net work of viscous stresses (third term), plus the net work done by body forces to increase kinetic energy (fifth term), minus the viscous dissipation (fourth term). Re-writing the gravitational body force term, integrating over a streamtube control volume,  $V$ , and expressing the vector gradient in the streamwise direction,  $s$ , for steady-state flow:

$$\int_V \rho V \frac{\partial}{\partial s} \left( \frac{1}{2} V^2 + \frac{p}{\rho} + gz \right) dV = \int_V (\nabla \cdot \tau \cdot \bar{v}) dV - \int_V \tau : \nabla \bar{v} dV \quad (6)$$

The net viscous work term (first term on right side) is the work done by viscous stresses in the fluid element against the surroundings to change kinetic energy of the fluid.

More specifically, consider a control volume,  $A(ds)$ , of finite width in the cross-stream direction and differential length in the streamwise direction. Integrating over this control volume and assuming a uniform mass flow rate through the streamtube encompassing the control volume, it can be shown that:

$$\dot{m} \int_1^2 d \left( \frac{1}{2} V^2 + \frac{p}{\rho} + gz \right) = \int_V \nabla \cdot \tau \cdot \bar{v} dV - \int_V \tau : \nabla \bar{v} dV \quad (7)$$

The last term on the right side refers to viscous dissipation within the control volume. It reduces mechanical energy by dissipating mechanical energy to internal energy.

The viscous dissipation represents a loss term, which can be related to the local rate of entropy production based on Equation 2. Performing that substitution and comparing to Bernoulli's equation, where  $T$  is the local temperature within volume  $V$ , it can be shown that the head loss becomes:

$$h_l = \frac{1}{\dot{m}} \int_V T \dot{P}_s dV \quad (8)$$

Alternatively, this result can be expressed in terms of the local rate of exergy destruction,  $\dot{X}_d$ , due to friction irreversibilities of viscous dissipation, i.e.:

$$h_l = \frac{1}{\dot{m}} \int_V \dot{X}_d dV \quad (9)$$

The locally measured entropy production and temperature are multiplied by the discrete volume outlined in the spatial PIV grid of measured velocities. For internal flows, the result represents a useful alternative to conventional loss parameters. It provides a generalized form of flow losses and a standardized metric, from which the energy efficiency of any flow device can be characterized.

Analogous results could be derived for external flows, but internal friction coefficients would be replaced by a drag coefficient.

In contrast to past methods characterizing flow losses through global empirical coefficients, this approach allows local tracking of flow losses. As mentioned earlier, entropy production serves as a more useful variable for tracking such losses, rather than primary variables such as pressure. For example, entropy production encompasses all flow irreversibilities (thermal, friction, electromagnetic and so forth), unlike pressure, which may be de-coupled from temperature under certain flow conditions. Also, the units of exergy destruction ( $\text{W}/\text{m}^3$ ) can be more readily converted to lost revenue in fluid systems. Reduced destruction of exergy is a common objective, but changes of individual flow variables are problem dependent.

For example, higher pressure losses of added baffles lead to a desirable increase of heat transfer rates in a heat exchanger. On the other hand, reduced pressure losses are needed in pipe flows, as they entail lower pumping input power. Thus, tracking local pressure changes does not generally identify a problem area. On the other hand, lower entropy production rates represent a more general objective. It can be more valuable than tracking end-to-end pressure losses, since the desired overall performance can be improved by re-designing locally. In the next section, sample results of flow irreversibilities will be presented and equivalence between conventional loss parameters and the entropy-based metric will be discussed.

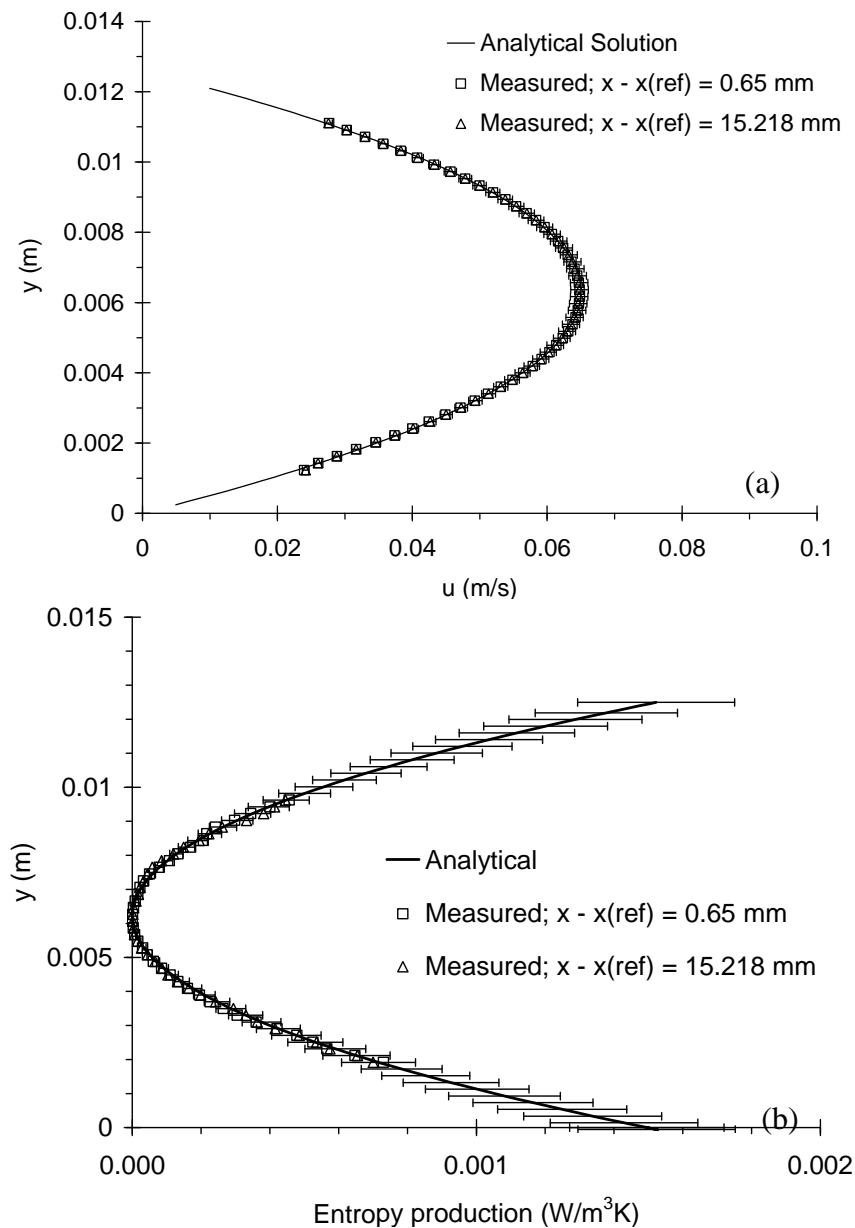
## 5. Results and Discussion

In this section, the following two application problems are considered: (i) channel flow between parallel plates and (ii) two-dimensional laminar flow in a cross-sectional plane above a magnetic stirrer. In the first case, validation of the experimental technique of flow irreversibility measurement is performed through comparisons with analytical solutions. The second problem has been documented previously [8,20], but this article extends those past studies to irreversibility measurements.

### 5.1. Parallel Channel Flow Problem

The conversion algorithm for measured entropy production and flow irreversibilities was validated against analytical entropy production results for water flow in a parallel channel. As described previously, the experiment was carried out in a water tunnel seeded with 5 micron diameter polyamide particles. The channel is 12.6 mm high, 60 cm wide and 2 m long. Flow measurements were performed at different streamwise ( $x$ ) locations, in order to verify that fully developed conditions were reached.

The measured velocity and entropy production are compared with the corresponding analytical solutions in Figure 2a,b, respectively, at  $\text{Re}_H = 518$ . The analytical solution for laminar flow between parallel plates is a well-known quadratic profile, which is analogous to the Poiseuille velocity profile in pipe flows. In Figure 2a, the deviations of measured velocities lie within 1.2% of the analytical values. The maximum difference between the measured entropy production and the analytical result is 6.6%. These results provide useful validation of the post-processing and conversion algorithm for entropy production due to friction irreversibilities.

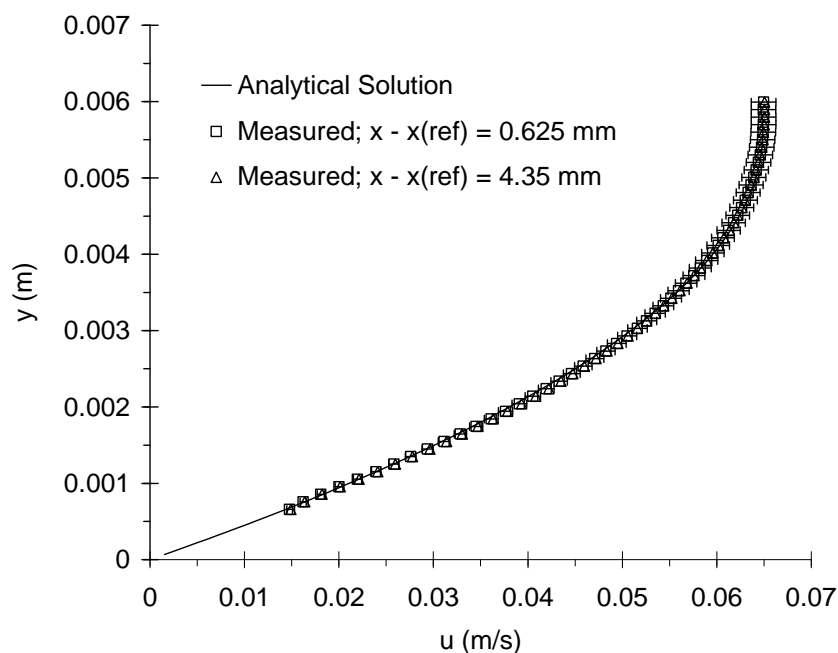
**Figure 2.** (a) Velocity (error bars at 2%) and (b) entropy production (error bars at 15%).

For this problem, thermal irreversibilities are neglected, since the flow is effectively isothermal. In Figure 2a,b, a reference point,  $x(\text{ref})$ , designates a location where analytical solutions of the laminar boundary layer development imply fully developed conditions within the parallel channel. Measurements at two different locations downstream of this point (0.65 mm and 15.218 mm) are taken, in order to confirm that both profile shape and magnitude are preserved. The measured results show close agreement between both downstream points, thereby providing useful evidence of fully-developed conditions. In many wall-bounded flows, including this channel flow problem, the highest entropy production is located at the wall, where the largest spatial gradients of velocity and temperature are encountered.

Near-wall measurements of velocity and temperature are often most difficult. In particular, limitations of camera resolution and particle tracking near the wall arise with PIV technology. Attempts were made to focus the particle tracking and image processing as close to the wall as

possible. In Figure 3, measured velocities were obtained within a distance of 1 mm from the wall. It can be observed that close agreement between measured velocities and the analytical solution is obtained close to the wall. Both places at different streamwise locations (i.e., 0.625 mm and 4.35 mm from the reference point) yielded close agreement, so near-wall measurements were determined to be independent of the x-position under fully-developed conditions.

**Figure 3.** Near-wall velocity measurements (error bars at 2%).



With regards to entropy production, Figure 4 shows close agreement between the analytical solution and measured data. Closer agreement is observed than results predicted by a detailed measurement uncertainty analysis (see appendix). However, the error increases closer to the wall, so the reported experimental uncertainties give a maximum bound on expected errors up to the wall. A surface plot of measured entropy production in the channel is depicted in Figure 5.

In Figures 4–5, it can be observed that the entropy production becomes zero at the center-line and it reaches a peak value at the wall. The local head loss coefficient can be derived from these results, after multiplying the local entropy production rate by the bulk temperature and volume size corresponding to the discrete PIV grid points, as well as dividing by the channel mass flow rate. This result represents the local exergy destruction per unit mass flow.

It is useful to verify that this loss coefficient yields the same result as the standard loss coefficient for channel flows. For incompressible, fully developed flow between parallel plates of length  $L$  and spaced  $2W$  apart, the velocity profile can be expressed as:

$$u(y) = \frac{W^2 \Delta p}{2\mu L} \left[ \left( \frac{y}{W} \right)^2 - 1 \right] \quad (10)$$

**Figure 4.** Near-wall measurements of entropy production (error bars at 15%).

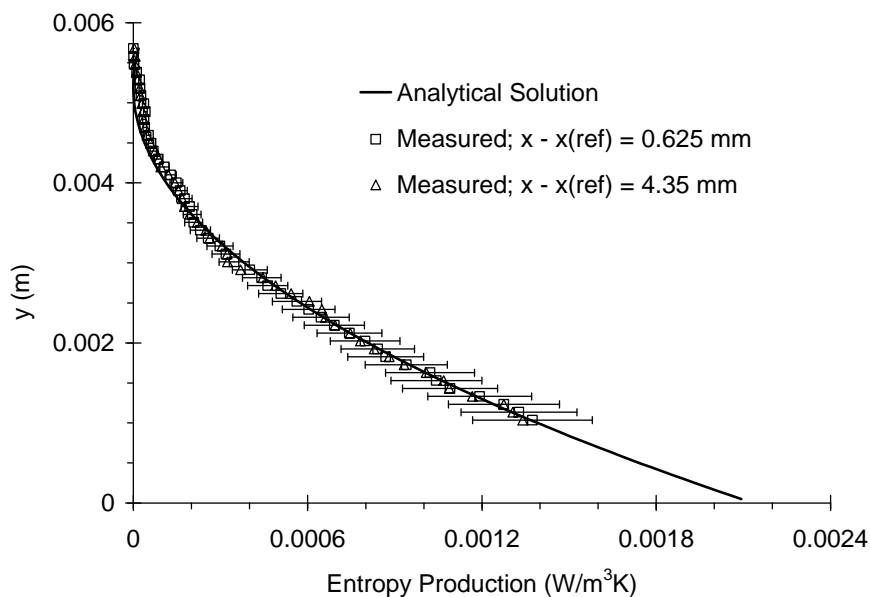
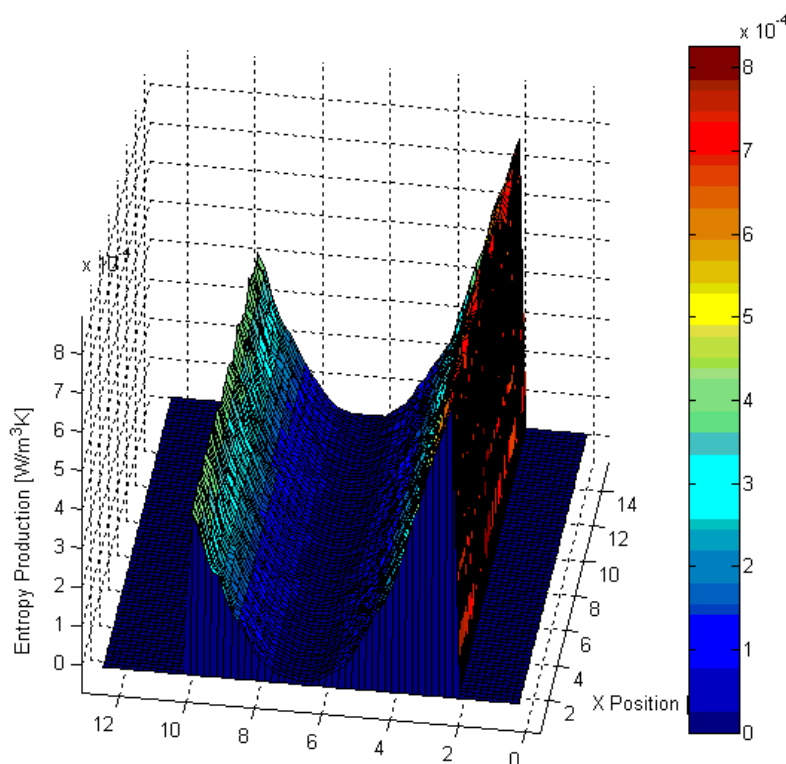


**Figure 5.** Surface plot of measured entropy production in channel flow.



Using Equations 2 and 10 to evaluate the entropy production rate, multiplying by temperature and integrating the result of Equation 8 across the channel yields the following head loss:

$$h_l = \frac{1}{\dot{m}} \int_{-w}^w \mu \left( \frac{\partial u}{\partial y} \right)^2 L dy = \frac{\Delta p}{L} \tag{11}$$

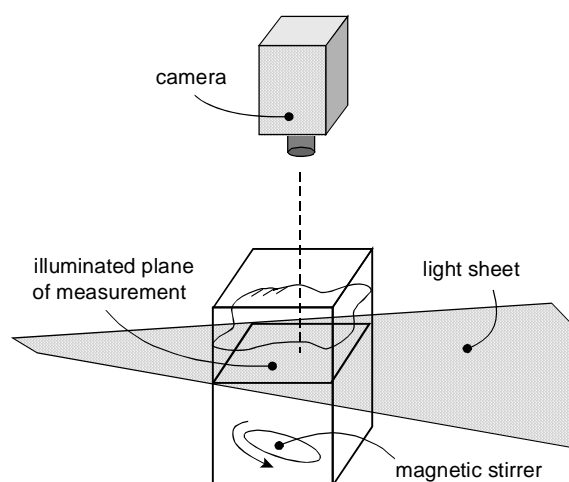
Thus, the entropy based formulation of Equation 8 for channel flow reduces to  $\Delta p / L$ , which is the expected head loss in undergraduate textbooks for viscous flow between two wide flat plates. More

generally, the exergy based loss coefficient (summed over the entire spatial domain) becomes equivalent to the corresponding global loss parameter in undergraduate fluid mechanics textbooks. For example, the loss coefficient for a tee junction in undergraduate textbooks would be equivalent to the summed exergy destruction per unit mass flow over the spatial domain encompassing the tee junction. There is a significant advantage of this exergy based technique, since the exergy destruction can be measured locally, thereby providing additional local variation of the loss coefficient.

### 5.2. Magnetic Stirring Tank Problem

This problem examines laminar fluid motion induced by a magnetic stirrer in a cuvette cube [8,20]. A schematic of the magnetic stirrer and pulsed light sheet for PIV is shown in Figure 6.

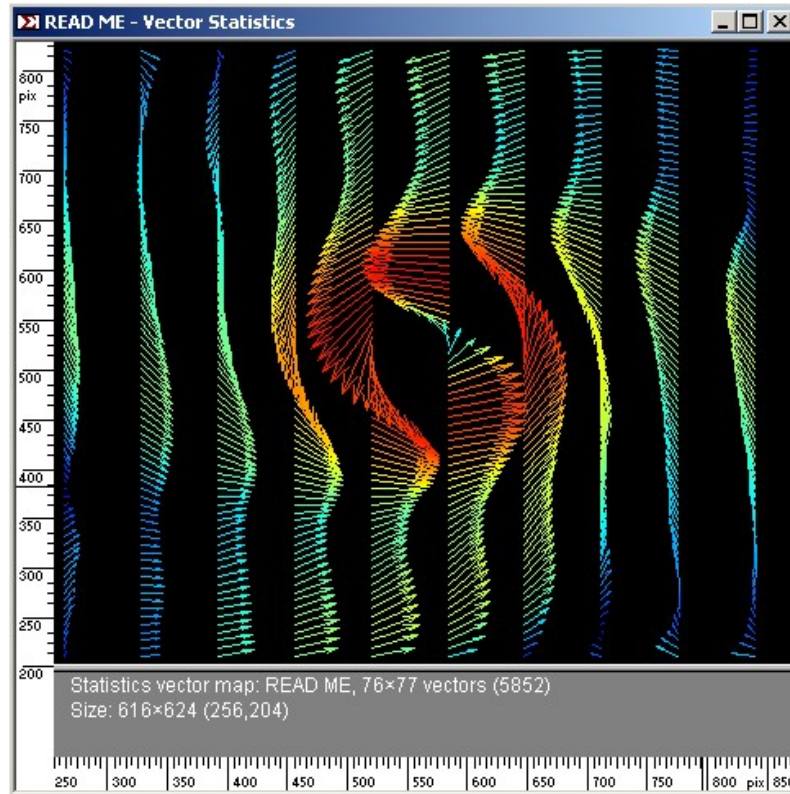
**Figure 6.** Schematic of magnetic stirrer.



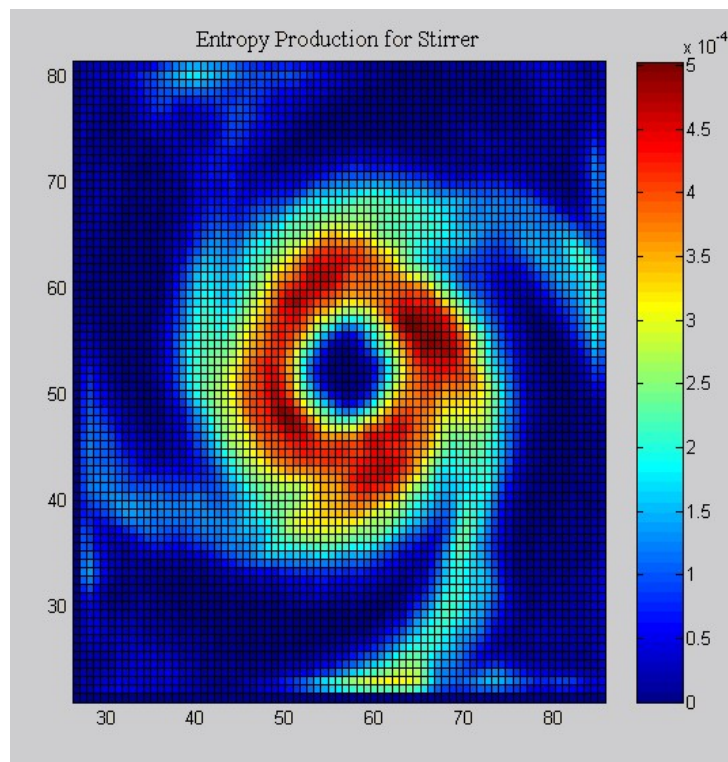
Magnetic stirrers are commonly used in chemical processing laboratories. Based on the rotational speed of the stirrer and the operating conditions of the camera (running at 30 Hz), each rotation was resolved with 20 image frames. The cube side length is 6 cm and the double-pulsed Nd:Yag laser operates at 10 mJ per pulse. The light sheet enters the cuvette about 5 mm below the free surface and well above the plane of mixing. Due to this illumination above the mixing plane and a smooth surface stirrer, two-dimensional steady flow is viewed in the observation plane. One thousand double-pulsed recordings were used to measure detailed flow characteristics of both the core vortex and merging of smaller tip vortices from the tip of the magnetic stirrer. Figure 7 illustrates the measured velocity field within the plane of the light sheet used to illuminate the 50  $\mu\text{m}$  seeding particles. Based on this velocity field, entropy production rates of the in-plane motion are determined and plotted in Figures 8 and 9. As expected, the regions of high mixing yield the highest rates of entropy production. Stirring tanks contain inlet and outlet ports, so the inlet mass flow rate would be used when calculating the exergy based loss coefficient in Equation 9 under steady-state conditions. In this example, the practical application of a magnetic stirrer typically involves mixing of chemicals to provide uniform mixtures. As a result, uniformly distributed magnitudes of entropy production may be desired to maximize

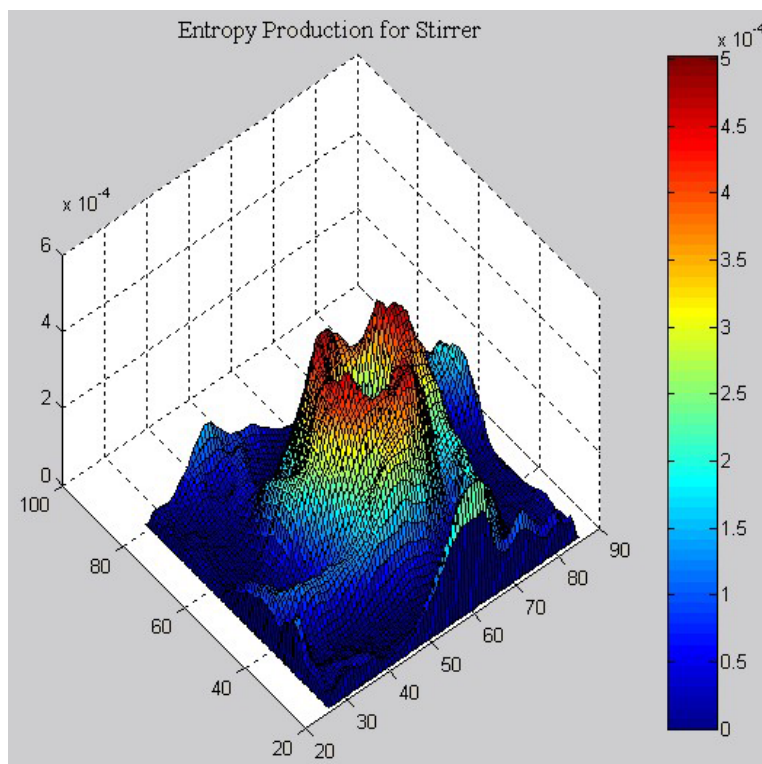
mixing. Based on the measured entropy production rates, the impeller could be re-designed to extend the diffusive effects induced by mixing.

**Figure 7.** Measured velocity field (note: maximum velocity of 5.5 cm/s).



**Figure 8.** Contours of entropy production ( $\times 10^{-4} \text{ W/m}^3\text{K}$ ).



**Figure 9.** Surface profiles of entropy production ( $\times 10^{-4}$  W/m<sup>3</sup>K).

Although maximum entropy production may lead to higher mixing, it also consumes additional input power. If energy efficiency of mixing becomes an important design criterion, then lower total entropy production may be needed, with more uniformly distributed rates of entropy production. In that case, re-design of the tank geometry could provide such compromised objectives. Alternatively, the type, size, placement and rotational speed of the impellers could be changed, in view of reducing entropy production and local loss coefficients. For example, the surface plot of entropy production in Figure 9 is highly non-uniform. Smoothing of that surface and lower magnitudes will produce more uniform mixing, while consuming lower input power.

By summing the local entropy production measurements, the results provide a useful basis from which the energy efficiency of any device can be characterized. For example, based on the First Law, the thermal effectiveness of a heat exchanger is defined differently than a water heater's efficiency, while still different than a diffuser's efficiency, and so on. As a result, it is difficult for regulatory or government agencies to identify a standard way of identifying any device's energy wastefulness. In contrast, local or summed entropy production rates could provide an alternative standard quantity that is directly related to the efficiency of any energy consuming or producing device.

The previous examples represent specific applications, while many other potential applications of entropy measurement technology are envisioned. Some other examples of industrial applications include aerospace, automotive, power generation, turbomachinery, sprays, combustion, indoor ventilation, processing industries and other mixing processes. Spatial tracking of exergy based loss coefficients could allow designer to re-configure components locally, thereby improving overall system performance.

## 6. Conclusions

This paper developed an experimental technique for measuring local flow irreversibilities and entropy production. Problem areas could be identified, so that engineering devices are re-designed locally to reduce entropy production and improve system efficiency. Furthermore, exergy based loss coefficients provide useful alternatives to conventional global loss parameters, such as the pressure recovery coefficient. Indirectly measured entropy production and the resulting exergy based loss coefficients in laminar channel flow show close agreement with analytical solutions. Also, measured flow irreversibilities in a magnetic stirring problem show irregular mixing patterns near the stirrer tips. Energy of fluid motion loses a certain quality when entropy is produced. As future technologies become more complex in their consumption and conversion of energy, such as jet engines pressing to the limits of maximum performance, the full impact of the Second Law will become increasingly important for reaching the desired technological goals.

## Acknowledgements

Financial support of this research from the Natural Sciences and Engineering Research Council of Canada, University Industry Liaison Office (University of Manitoba) and a University of Manitoba Graduate Fellowship (O. B. Adeyinka) are gratefully acknowledged. Also, helpful suggestions from Robert Petterson, Janet Scholz (University of Manitoba) and Cliff Weissman (Dantec Dynamics) are appreciated. Research laboratory infrastructure support was received from CFI (Canada Foundation for Innovation) and WED (Western Economic Diversification).

## Appendix — Measurement Uncertainties

Measurement errors were assessed based on the AIAA standard [21]. In that procedure, the total error is a sum of the bias component,  $B$ , and a precision component,  $P$ . For the measured velocity,  $U$ , its bias error is related to the elementary bias errors based on the sensitivity coefficients, i.e.,

$$B_U^2 = \eta_{\Delta s}^2 B_{\Delta s}^2 + \eta_{\Delta t}^2 B_{\Delta t}^2 + \eta_{L_o}^2 B_{L_o}^2 + \eta_{L_i}^2 B_{L_i}^2 \quad (\text{A1})$$

where the sensitivity coefficients are defined as  $\eta_\chi = \partial U / \partial \chi$ . Manufacturer's specifications of the elementary bias limits were obtained. By combining the contributions of each bias error and the sensitivity coefficient, a velocity error of 0.76% was obtained.

The precision error ( $P$ ) for measurements of  $N$  samples is given by

$$P = \frac{t\sigma}{N} \quad (\text{A2})$$

where  $t$  is the confidence coefficient (equaling 2 for a 95% confidence interval) and  $\sigma$  is the standard deviation of the sample of  $N$  images. Calculated values of the standard deviation along the center-line and the near-wall region are 15% and 33%, respectively, thereby yielding precision limits of 0.67% and 1.55% for those regions. As a result, the total uncertainty of measured velocity in the middle of the channel and the near-wall region are 1.4% and 2.2%, respectively.

Using these velocity results, the measurement error of entropy production for near-isothermal flows can be estimated based on the following data reduction equation for fully developed flow,

$$P_s = \frac{\mu}{T} \left( \frac{\Delta u}{\Delta y} \right)^2 \quad (\text{A3})$$

A similar procedure is performed with bias and precision errors involving entropy production, so that the total error becomes

$$\varepsilon_{P_s}^2 = \eta_{\Delta U}^2 \varepsilon_{\Delta U}^2 + \eta_{\Delta y}^2 \varepsilon_{\Delta y}^2 \quad (\text{A4})$$

The maximum total uncertainty of measured entropy production was calculated to be 11.67% at a point of 3 mm from the bottom wall. This estimate represents the maximum error bound within a 95% confidence interval. Comparisons between measured and analytical results in Figures 2–4 show less error closer to the center-line of the channel.

## References

1. Bejan, A. *Entropy Generation Minimization: The Method of Thermodynamic Optimization of Finite-Time Systems and Finite-Time Processes*, CRC Press LLC: Boca Raton, FL, USA, 1996
2. Naterer, G.F. *Heat Transfer in Single and Multiphase Systems*. CRC Press LLC: Boca Raton, FL, USA, 2002.
3. Camberos, J.A. Revised Interpretation of Work Potential in Thermophysical Processes. *AIAA J. Thermophys. Heat Transfer* **2000**, *14*, 177–185.
4. Roth, B.; Mavris, D. A Method for Propulsion Technology Impact Evaluation Via Thermodynamic Work Potential. AIAA Paper 2000-4854, In *Proceedings of the 8th AIAA/USAF/NASA/ISSMO Symposium on Multidisciplinary Analysis and Optimization*, Long Beach, CA, USA, 2000.
5. Moorhouse, D.J.; Suchomel, C.F. Exergy Methods Applied to the Hypersonic Vehicle Challenge. AIAA Paper 2001-3063, In *Proceedings of the 32nd AIAA Plasmadynamics and Lasers Conference, 4th Weakly Ionized Gases Workshop*, Anaheim, CA, USA, June 11–14, 2001.
6. Azar, K.; Russell, E.T. Effect of Component Layout and Geometry on the Flow Distribution in Electronics Circuit Packs. *ASME J. Electron. Packag.* **1991**, *113*, 50–57.
7. Naterer, G.F.; Glockner, P.S. Pulsed Laser PIV Measurements and Multiphase Turbulence Model of Aircraft Engine Inlet Flows. AIAA Paper 2001-3032, In *Proceedings of the AIAA 31st Fluid Dynamics Conference*, Anaheim, CA, USA, June 11–14, 2001.
8. Dantec D. Animation of a Time-Resolved Flow Using New FlowMap PIV Features. *Dantec Newslett.* **1999**, October 11.
9. Bejan, A., Ledezma, G.A. Thermodynamic Optimization of Cooling Techniques for Electronic Packages. *Int. J. Heat Mass Transfer.* **1996**, *39*, 1213–1221.
10. Landauer, R. Irreversibility and Heat Generation in the Computing Process. *IBM J.* **1961**, 183–191.
11. Naterer, G.F.; Camberos, J.A. Entropy and the Second Law in Fluid Flow and Heat Transfer Simulation. *AIAA J. Thermophys. Heat Transfer* **2003**, *17*, 360–371.

12. Majda, A.; Osher, S. Numerical Viscosity and the Entropy Condition. *Commun. Pure. Appl. Math.* **1979**, *32*, 797–838.
13. Merriam, M.L. Towards a Rigorous Approach to Artificial Dissipation. AIAA Paper 89-0471, In *Proceedings of the 27th Aerospace Science Meeting*, Reno, NV, USA, January 1989a; pp. 9–12.
14. Merriam, M.L. *An Entropy Based Approach to Numerical Stability*. NASA Report No. TM-101086, NASA Ames Research Center, Moffett Field, CA, USA, 1989b.
15. Naterer, G.F. Constructing an Entropy-Stable Upwind Scheme for Compressible Fluid Flow Computations. *AIAA J.* **1999**, *37*, 303–312.
16. Hughes, T.J.R.; Franca, L.P.; Mallet, M. A New Finite Element Formulation for Computational Fluid Dynamics: I. Symmetric Forms of the Compressible Euler and Navier - Stokes Equations and the Second Law of Thermodynamics. *Comput. Method. Appl. Mech. Eng.* **1986**, *54*, 223–234.
17. Adeyinka, O.B.; Naterer, G.F. Apparent Entropy Production Difference with Heat and Fluid Flow Irreversibilities. *Numer. Heat Transfer B* **2002**, *42*, 411–436.
18. Nellis, G.F.; Smith, J.L. Entropy-Based Correction of Finite Difference Predictions. *Numer. Heat Transfer B* **1997**, *31*, 177–194.
19. Naterer, G.F.; Schneider, G.E. Use of the Second Law for Artificial Dissipation in Compressible Flow Discrete Analysis. *AIAA J. Thermophy. Heat Transfer* **1994**, *8*, 500–506.
20. Hammad, K.J.; Papadopoulos, G. Phase-Resolved PIV Measurements in a Stirred Tank. In *Proceedings of the AIChE Conference*, Los Angeles, CA, USA, Nov. 2000; pp. 12–17.
21. AIAA Standard S-071-1995, *Assessment of Experimental Uncertainty with Application to Wind Tunnel Testing*, American Institute of Aeronautics and Astronautics: Washington, DC, USA, 1995.

© 2009 by the authors; licensee Molecular Diversity Preservation International, Basel, Switzerland. This article is an open-access article distributed under the terms and conditions of the Creative Commons Attribution license (<http://creativecommons.org/licenses/by/3.0/>).